Scientific Reports

https://doi.org/10.1038/s41598-026-38314-z

Article in Press

Cutting parameter-tool material interaction on PcBN tool wear behaviour in ductile iron machining

Received: 17 July 2025

Accepted: 29 January 2026

Published online: 17 February 2026

Cite this article as: Wang P., Li X., Jiu Y. *et al.* Cutting parameter-tool material interaction on PcBN tool wear behaviour in ductile iron machining. *Sci Rep* (2026). https://doi.org/10.1038/s41598-026-38314-z

Pengfei Wang, Xiaojing Li, Yongtao Jiu, Huiming Yin & Yingbo Zhang

Cutting Parameter-Tool Material Interaction on PcBN Tool Wear Behaviour in Ductile Iron Machining

Pengfei Wang[1] , Xiaojing Li[2]*,Yongtao Jiu[1] ,Huiming Yin[1] Yingbo Zhang[2]
（1. Ningbo Zhongji Songlan Cutting Tool Technology Co., Ltd, Ningbo 315700, China;
2.Hebei Petroleum University of Technology, 2 Xueyuan Road, Shuangqiao District, Chengde, Hebei Province, Chengde 067000, china. *Email: lixiaojingre@163.com）

Abstracts: In response to the increasing requirements for the processing quality and precision of ductile iron parts under the trend of automotive lightweighting and emission reduction,this study systematically investigated the wear behavior and cutting parameter optimization method of polycrystalline cubic boron nitride (PcBN) tools when machining ductile iron.By designing cutting experiments, the influence of different cutting parameters and tool materials on the service life of PcBN tools was analyzed.Based on the observation of the wear morphology throughout the tool’s life cycle, the failure evolution mechanism of PcBN tools with different compositions was revealed.With the help of microscopic characterization techniques, it was identified that abrasive wear, chemical wear, and adhesive wear are the main wear mechanisms of the tools. The results show that:Type B tools with cermet binders exhibit excellent cutting performance and a longer service life when machining ductile iron; under the optimized condition with a cutting efficiency of 15.04cm^3/min, a good balance between machining efficiency and tool life was achieved. Cutting speed, feed rate, and cutting depth have a significant impact on tool life, and there are obvious differences in the wear mechanisms of tools with different compositions. Based on the experimental data, a tool life prediction model was established through multiple linear regression. This model integrates real - time sensor data, can dynamically calculate the remaining life and health status, and achieve wear warning. This study provides theoretical and technical support for improving the efficiency and service life of PcBN tools in machining ductile iron, and points the way for the composition design of the next - generation cermet - bonded PcBN.

Keywrods: PcBN Wear Mechanisms； Ductile Iron Machining； Wear Mechanism；Life Prediction.

1.Research Background

As the "heart" of automobiles, both the engine and the drive motor widely employ high-performance ductile iron for their key structural components.Specifically,typical applications of ductile iron include the crankshaft,cylinder block,and cylinder head of the engine,as well as the

housing, end cover,and bearing seat of the drive motor.With mechanical properties approaching those of steel,this material has become a mainstream choice for critical structural components in automotive powertrains.Typical applications include crankshafts for small and medium-sized engines,which replace traditional forged steel,as well as widely adopted housings for drive motors.In the field of mechanical machining,polycrystalline cubic boron nitride (PcBN) cutting tools exhibit significant advantages for green manufacturing applications,including high-speed cutting and hard turning, owing to their high hardness, excellent thermal stability,and chemical inertness.

It is noteworthy that, in addition to achieving ‘turning instead of grinding’ by increasing cutting parameters,employing tools with specialised geometric cutting edges—such as wiper tools—is equally an effective approach to enhancing machined surface integrity and thereby substituting grinding processes. Research indicates that when milling cast iron,novel inserts featuring convex finishing edges achieve superior surface roughness compared to conventional inserts operating at low feed rates (0.1 mm/tooth),even under high feed conditions (0.4 mm/tooth). This approach enhances production efficiency by over fourfold while improving surface finish by approximately 35%[1].Furthermore, during hard turning of AISI D2 steel, synergistic optimisation of the finishing insert's cutting edge preparation, workpiece hardness, and cutting parameters has been demonstrated as crucial for simultaneously ensuring high surface quality and tool life[2]. These studies broaden the technical scope of ‘turning instead of grinding’ and emphasise the pivotal role of tool microgeometry in achieving high-performance machining.

A series of in-depth studies on machining ductile iron with PcBN tools has been reported in the literature.Regarding tool materials, tools with high cBN content (≥90 wt%) demonstrate superior impact resistance during interrupted cutting of ductile iron;Research by Zou et al. indicates that metal additions such as W and Al suppress diffusion-chemical wear,while high-entropy ceramic (HEA-ceramic) binders have been proven to simultaneously enhance both hardness and fracture toughness[3].In surface modification techniques,Geng et al. utilised laser processing to create micro-pitted textures on PcBN chamfered surfaces. They discovered that rationally distributed textures reduced tool-chip contact length by 18%, minimised chip adhesion, and extended tool life by 22%[4].Uhlmann et al. employed ECR-MPCVD to deposit a 2μm cBN coating on Si_3N_4 substrates, achieving a 40% cost reduction. During high-speed turning of ductile iron, the coating exhibited a wear rate below $1\times10^{-3}mm^3(N\bullet m)^{-1}$[5].Concerning wear mechanisms and process optimisation,systematic experiments revealed the critical influence of cutting speed.Geng et al. found that within the cutting speed range of 250–350 $m\bullet min^{-1}$,the primary failure sequence for PcBN was:crescent-shaped pitting on the rake face→micro-chipping at the

cutting edge→high-cycle fatigue cracking at the tool tip.When v exceeded 400 m min^{-1},diffusion wear intensified,resulting in an exponential decline in tool life[6].Peicheng M et al. developed a life model based on the energy-threshold concept,which predicted errors of less than 15%,providing theoretical support for process window selection[7].Tu Luqiang et al.[8] successfully deposited a 2μm thick cBN coating on Si_3N_4 tools using ECR-MPCVD technology combined with a boron-doped diamond (BDD) transition layer,addressing the high cost issue of conventional cBN tools. Xie Hui[9] investigated the effects of high-temperature,high-pressure sintering on PcBN performance.Results indicated that horizontal planetary ball milling could refine cBN particles to 4–8μm,while ultra-high-pressure sintering (5–6 GPa) promoted plastic deformation and densification of particles,though potentially inducing crack defects. Li Jian[10] synthesised SiC whiskers via in-situ reaction technology. Combined with spark plasma sintering (SPS),this significantly enhanced PcBN toughness and sintering efficiency, achieving a composite flexural strength of 406 MPa.Boing et al.[11] proposed a method for predicting the hard turning tool life of PCBN tools based on three-dimensional wear parameters.By measuring wear volume during the early stages of tool life (≤25%) using a focused variation microscope and combining this with least squares methods to calculate wear rates,the resulting model achieved life predictions with an error margin below 4% under commonly used high cutting speeds in industry.This approach significantly reduced experimental testing time.Khadka,Sujan et al.[12] systematically reviewed modelling and monitoring techniques for cutting tool life,highlighting that future research will focus on developing hybrid models integrating empirical and analytical approaches, constructing more comprehensive datasets,and ultimately advancing adaptive,self-learning tool performance prediction systems and integrated monitoring technologies to drive optimisation of manufacturing efficiency and cost-effectiveness.Wu Mingyang et al.[13] established a cutting simulation model for the rake face wear of PCBN tools.They analysed the effects of high-pressure cooling on cutting forces, temperatures,and residual stresses.A tool life prediction model was developed using a GA-BP neural network.The model's generalisation capability was evaluated through six-fold cross-validation.Results indicate that high-pressure cooling effectively reduces cutting forces and temperatures.Furthermore, as the rake face wear width increases,the force-heat load exhibits an upward trend.These endeavours have advanced PcBN tool technology across multiple dimensions, including material preparation,structural design and process experimentation,and service life prediction.

Despite the aforementioned progress,it must be recognised that fundamental scientific issues—such as tool wear mechanisms,cutting force models,and parameter influence patterns—are universal across different tool materials (e.g., cemented carbide, ceramics).Drawing upon broader research

findings can provide valuable perspectives for deepening our understanding of PcBN tool wear behaviour.For instance, studies on grooved-edge tools demonstrate that reducing the actual tool-workpiece contact length through design can significantly decrease cutting forces, power consumption,and specific cutting energy by 7–17%.This provides direct evidence for understanding the mechanism by which edge geometry optimisation enhances machining efficiency and sustainability[14].Furthermore, integrated experimental and numerical simulation studies examining the influence of micro-geometric parameters of the finishing edge (such as arc radius and transition angle) have become precise and practical methods for optimising tool performance and predicting machining behaviour[15].Concurrently, systematic investigations into the effects of high-pressure cooling and cutting parameters (speed, feed) on surface roughness[16] underscore the significance of interactions between cooling conditions and process parameters. These studies from other tool material systems collectively highlight the necessity for multi-factor coupled analysis of ‘cutting parameters-tool geometry-machining environment’, laying the foundation for establishing a systematic experimental and analytical methodology in this research.

In contrast,within the specific domain of ductile iron machining, existing research on PcBN tools exhibits three prominent limitations that warrant further investigation:

Under equivalent operating conditions,the tool life of PcBN cutting ductile iron is merely 5–10% that achieved with grey iron,with a lack of systematic analysis linking microstructural differences (‘ductile-ferritic/pearlitic’) to wear mechanisms;Most studies focus on single factors (speed or binder),exhibiting weak correlation among cutting parameters and lacking unified criteria for process optimisation;Although metal-ceramic composite bonds have been proposed, research into their synergistic effects (‘metal phase toughening-ceramic phase heat resistance’) remains nascent, with insufficient verifiable data.

Therefore,this study proposes to:

1.Conduct multi-factor orthogonal turning experiments to establish a significance ranking of speed-feed-depth of cut on tool life, providing a recommended parameter range for high-speed finish turning of ductile iron;

2.Track wear morphology evolution throughout the entire tool life cycle, quantitatively comparing failure pathways between 80% cBN-Co bonded and 90% cBN-HEA bonded tools;

3.Characterise the interface diffusion layer using FIB-SEM, EDS and TEM, combined with microstructural analysis to reveal the diffusion-fatigue synergistic wear mechanism, providing theoretical foundations for the composition design of next-generation metal-ceramic bonded PcBN tools.

2.1 Experimental Conditions

2.1.1 PcBN Tool Parameter Setting

In this experiment,three types of polycrystalline cubic boron nitride cutting tools (denoted as tool A，tool B and tool C) were selected,and their micromorphologies are shown in Fig.1.Tool A and B exhibited similar cBN contents and particle sizes.The cBN content in tool A (with metal binder),tool B (with cermet binder),and tool C was lower,with a wider cBN particle size distribution.The use of metal binders or appropriate alternative binders can reduce the sintering temperature/pressure while enhancing sintered body performance[17].The selected 80° diamond-shaped blade (Type C, Model CNGA120404) has the following parameters:0° rake angle, 0°clearance angle, 0° cutting edge inclination, 0.4 mm nose radius, 20°×0.2 mm negative chamfer,with passivation treatment.The specific cutting tool and tool holder are shown in Fig.2.Detailed parameters are listed in Tab. 1.

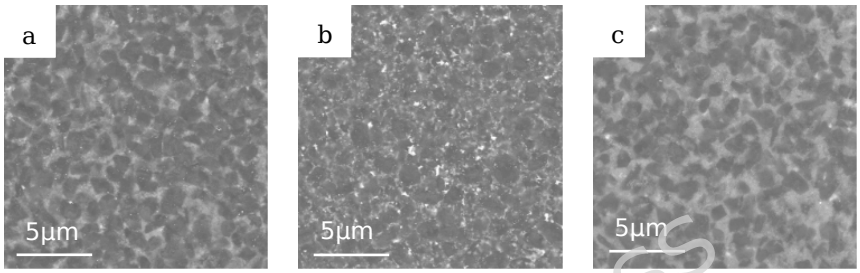

Fig.1 Micro-morphology of three cutting tools

（a） （b）

Fig. 2 Test tool (a) and test tool holder (b)

Tab. 1 Comparison of PcBN tools

Code	cBN content(%)	Grain size(μm)	Binder
Tool A	90	2-3	Metal
Tool B	83	2-3	Titanium carbide
Tool C	60	2-4	Titanium nitride

The workpiece material was ductile iron QT700, and its main chemical composition is listed in Tab. 2.The diameter of the workpiece was φ100 mm, and its length was 300mm. The tensile strength, yield strength is 700Mpa and 420MPa, elongation is 2%, and Brinell hardness (HB) is 250–350MPa, respectively.

Tab. 2 Chemical components of QT700(wt.%)

Element	C	Si	Mn	S	P
Mass Fraction	3.2	2.61	0.55	0.017	0.047

2.1.2 Experimental Machine Tools and Characterisation Instruments

A LBR-370-e CNC lathe was selected for the cutting test.The flank wear amount VB of the cutting tool was measured using a KEYENCE VHX-970 ultra-depth-of-field microscope.The morphology and surface elemental composition of the cutting tool were measured using a ZEISS EVO 10 scanning electron microscope with its built-in EDS energy-dispersive spectroscopy function.

3.Design of Experimental Method

3.1Determination of Initial Parameter Ranges

Systematic research on machining ductile iron with polycrystalline cubic boron nitride (PcBN) tools remains limited, resulting in a lack of unified standards for cutting parameters.Existing studies provide crucial guidance for establishing a feasible parameter window. It has been reported that PcBN tools exhibit extended tool life and reduced cutting forces within a cutting speed (v) range of 150 to 500 m/min[18].Furthermore, for economically viable machining, recommended ranges for the feed rate (f) and depth of cut (ap) are 0.1–0.4mm/r and ≤ 0.5mm, respectively[19]. The feed rate significantly influences workpiece surface roughness,and its increase generally elevates cutting force while causing the cutting temperature to first decrease and then increase[19, 20].Therefore,based on the aforementioned literature concerning PcBN machining of cast iron[18–20],the following parameter ranges—deemed conducive to achieving economically viable tool life—were selected as the foundation for this study: cutting speed v=150-500m/min, feed rate f=0.1-0.4mm/r, and depth of cut ap ≤0.5mm.

3.2 Factor-Level Design and Construction of the Experimental Matrix

Within the established parameter ranges, the number of levels for each factor in the orthogonal experiment was designed differentially,reflecting their anticipated influence complexity on the “turning instead of grinding” objective.Considering its complex,non-linear, and pronounced effects on tool life and overall machining performance, the cutting speed was assigned six levels to finely map its behavior.In contrast, within the confines of finish machining pertinent to the set goal, the effects of feed rate and depth of cut are more direct and predictable. Consequently,these two factors were each set at two levels.Specific level values were chosen to align with the “turning instead of grinding” requirement: depths of cut of 0.3mm and 0.4mm were selected to balance material removal rate with expected precision; feed rates were set to relatively low values to prioritize surface finish.To efficiently analyze the effects of these three factors and their potential interactions with a minimal number of trials, a mixed-level orthogonal array $L_{12}(6^1 \times 2^2)$ was employed ,includes one factor with six levels (X) and two factors with two levels each (Y, Z), comprising twelve experimental groups, each with one replicate. The corresponding experimental parameter combinations are

detailed in Tab. 3 and Tab.4

Tab.3 Horizontal table of orthogonal test factors

Levels	Cutting speed （m/min）	Feed rate（mm/r）	Depth of cut（mm）
	X	Y	Z
1	188	0.15	0.30
2	235		
3	294		
4	367	0.20	0.40
5	459		
6	573		

Tab. 4 Orthogonal test scheme

Experiment group	Level factors of each parameter			Experiment group	Level factors of each parameter		
	X	Y	Z		X	Y	Z
1	188	0.15	0.3	7	235	0.15	0.4
2	235	0.15	0.3	8	367	0.15	0.4
3	459	0.15	0.3	9	573	0.15	0.4
4	235	0.20	0.3	10	188	0.20	0.4
5	367	0.20	0.3	11	294	0.20	0.4
6	573	0.20	0.3	12	459	0.20	0.4

3.3Experimental Procedure

Under the specified experimental conditions, cutting tests were performed on three types of tools,followed by wear analysis and energy-dispersive spectroscopy of the tools.The detailed experimental procedure is outlined below:

(1)Wear Test

Before the formal cutting tests commenced, each tool was inspected visually and its geometric dimensions were verified to ensure compliance with the test specifications.The workpiece blanks were then subjected to preparatory surface machining to remove any casting skin, oxide scale, or deformation layers from prior processing, thereby ensuring consistent test conditions.

The wear test was conducted in accordance with predefined cutting parameters. Following the measurement guidelines recommended in ISO 3685:1993,the test was paused at intervals corresponding to an accumulated cutting length of approximately 700 m. At each interval,the insert was removed, and the wear on the flank face of the tool was observed and measured using a toolmaker’s microscope until the average flank wear width (VB) reached the specified tool-life criterion of 0.2 mm, marking the end of the tool’s service life.

(2) Wear Analysis

After testing, the micro-morphology of the worn regions on both the rake face and the flank face was examined by scanning electron microscopy to identify the dominant wear mechanisms. Energy-dispersive spectroscopy

(EDS) was then employed to analyze the chemical composition of the worn surfaces.The results were compared with the elemental composition of the unused tool material.By correlating changes in elemental distribution and concentration with the observed wear morphology,the underlying wear mechanisms were elucidated.

4.Test Results

4.1Life Analysis

As shown in Tab. 5 and Fig. 3,analysis of the cumulative cutting time for 12 tool groups when flank wear (VB) reached 0.2mm reveals two key findings:1) Under varying cutting parameters, all tools exhibit consistent trends in cutting time duration;2) tool B demonstrates a significant advantage in sustained cutting time.This performance superiority correlates with optimized material properties (e.g.,hardness/toughness balance) and geometric parameters, enabling enhanced wear resistance under current machining conditions.

Tab.5 Tool life under different test groups

Experiment group	Cutting Time (min)			Experiment group	Cutting Time (min)		
	Tool A	Tool B	Tool C		Tool A	Tool B	Tool C
1	45	52	55	7	12	21	16
2	12	13	17	8	10	12	11
3	9	10	10	9	9	10	10
4	15	17	18	10	16	39	25
5	10	11	12	11	10	12	13
6	9	9	10	12	10	10	10

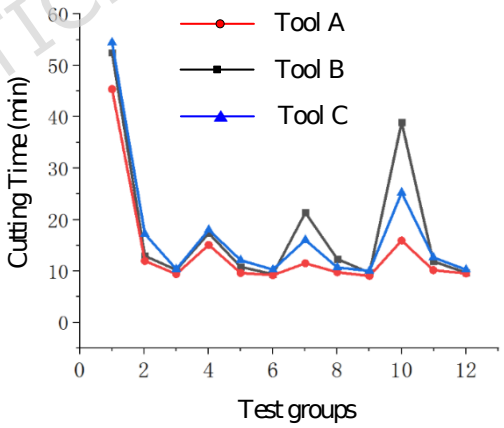

Fig. 3 Tool life under different test groups

To conduct an intuitive analysis of this changing trend, the concept of cutting efficiency was introduced. Based on the traditional cutting theory, the cutting efficiency Q (cm^3/min) can be calculated using the following formula 1：

$$Q = v \cdot f \cdot a_p \quad (1)$$

In the formula : v-cutting speed (m/min)， f-feed rate (mm/r)，a_p-depth of cut (mm)

Fig. 4 shows the tool cutting time for different machining efficiencies.Generally, an increase in the machining efficiency leads to a reduction in the cutting time of the tool.When considering only the cutting time of the tool, an efficiency of less than 10 cm^3/min should be selected. When the efficiency was below 15cm^3/min, the cutting time decreased sharply as the efficiency increases. Within the range of 15–20cm^3/min, the cutting times of Tools B and C first increased and then decreased. After comprehensive consideration, the efficiency interval of 15–20cm^3/min was the most favorable.

To further investigate these differences, considering the different cutting parameters, the cumulative volume of the material cut by the tool was calculated by multiplying the cutting efficiency by the cutting time. This volume is used as an accurate indicator for analyzing tool life. The results are presented in Fig. 5.The analysis indicated that tool B exhibited optimal cutting performance for ductile iron. When the cutting efficiency was 15.04cm^3/min,both the cutting efficiency and the longest tool life were considered. At this point, the cutting parameters are v = 188m/min, f = 0.2mm/r, and ap =0.4 mm. Substitute into formula (1) and calculate :

$$Q = 188000cm/min \times 0.02cm/r \times 0.04cm = 15.04cm^3/min \quad (2)$$

Tool C has more significant advantages in terms of cutting life at low (< 15cm^3/min) and high (> 25cm^3/min) cutting efficiencies and can be selected when the cutting efficiency is the primary objective.

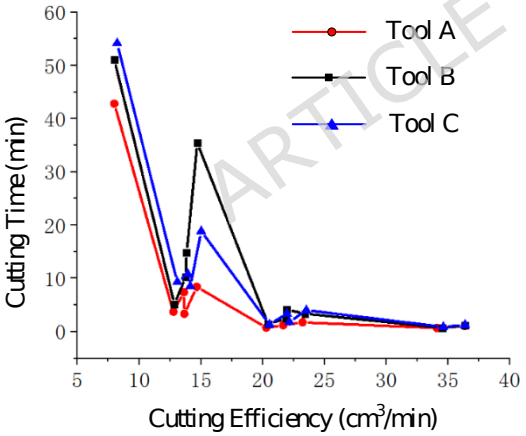

Fig. 4 Tool life with different machining efficiency

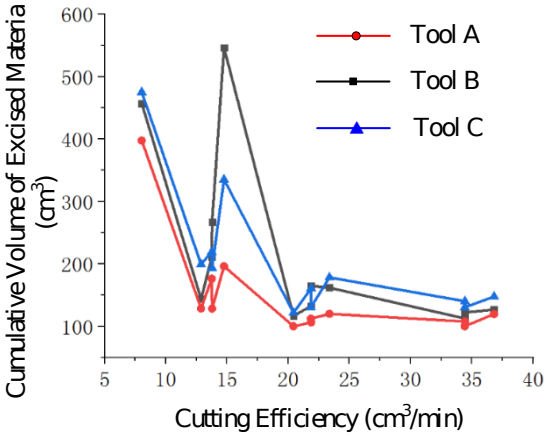

Fig. 5 Cumulative volume of excised material

During low cutting efficiency (<15cm^3/min),cubic boron nitride (cBN) content has a negligible impact on tool life. The service life of the low-cBN tool C is comparable to that of the high-cBN tool B,exceeding that of tool A by 20–100%. For high cutting efficiency (>25cm^3/min), tool C outperformed the high-cBN tools (tool A and tool B). For medium-speed cutting with similar cBN content and particle size, the titanium carbide-bonded tool B exhibited up to 80% longer life than that of the metal-bonded tool A.

As shown in Fig. 5, divergent tool life under identical machining

efficiency confirms the influence of cutting-triad parameters (speed, feed rate, and depth of cut) on longevity. To elucidate parameter dominance, experimental groups with matched efficiency (group4/7,group5/8,and group6/9) showed life variations despite identical cutting speeds.When the cutting depth was increased and the feed rate was decreased, the life of tool B was prolonged, whereas the lives of tool A and tool C were shortened. This indicates that the influence of the feed rate on the life of tool B is greater than that of the cutting depth. For Tools A and C, the cutting depth has a more significant influence, and tool A is particularly affected by the cutting depth, based on which, under the premise of the same cutting efficiency and controllable parameters, such as cutting force, cutting temperature, and surface roughness, to ensure machining quality and tool life, the cutting depth of tool B should be increased as much as possible, while a lower cutting depth should be selected for tool A and Tool C during cutting.

4.2Analysis of Tool Wear Process

During tool wear, crater wear develops on the rake face, whereas adhesion and diffusion wear manifest on the flank face. However, direct measurement of crater depth and flank-face abrasion grooves is challenging owing to positional inconsistencies, leading to significant measurement deviations. Consequently, the wear morphology and its distance from the cutting edge were adopted as the evaluation criteria. Based on the experimental longevity analysis in Section 4.1, taking into account the cutting efficiency and the longest tool life, the wear data of the rake face and flank face of test group 10 (v=188m/min，f=0.2 mm/r，ap=0.4 mm) were selected to analyze the wear process.

Fig. 6 depicts the evolution of crater wear on the rake faces of the three tools versus the cutting length. At the onset of cutting, the crater wear morphology exhibits irregular features that gradually regularize with the cutting progression, ultimately forming a characteristic half-moon shape. The wear propagated from the cutting edge toward the rake face interior, with the tool tip region demonstrating both the earliest onset and the most severe wear intensity.

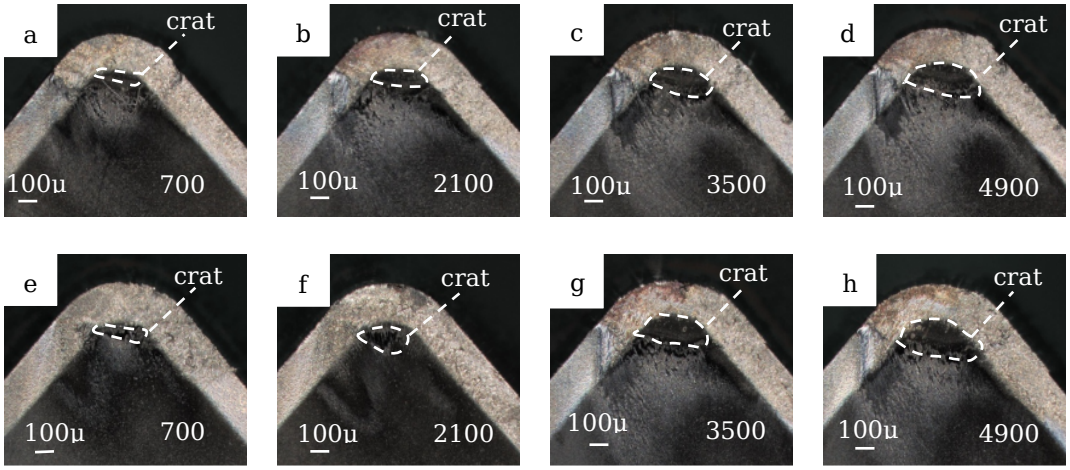

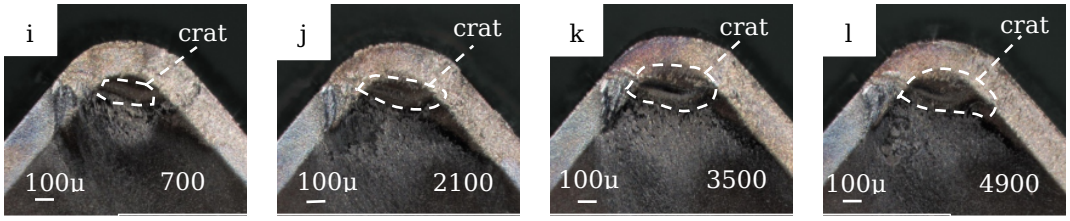

Fig.6 (a-d) tool B, (e-h) tool A, (i-l) tool C rake face wear

Under equivalent cutting lengths, tool C exhibited the most severe rake face wear, characterized by an extensive crater area and the farthest wear boundary from the cutting edge. Tool A demonstrated significant microchipping and pronounced built-up edge formation. Thermal discoloration and material delamination occur on the rake face of tool C owing to the elevated cutting temperatures. In contrast, Tools B and A showed milder crater wear, correlating with their higher cBN contents. Enhanced cBN concentration better preserves cutting edge integrity.However, Fig. 6 reveals comparable cutting-edge wear across all three tools. Micro-fragments from edge damage induce edge rounding and accelerate the wear progression. This wear divergence primarily stems from the differences in tool macro-hardness. Although high-hardness tools display reduced wear under specific conditions, the observed edge rounding effect demonstrates that wear resistance cannot be assessed solely by hardness, and practical machining operations require comprehensive consideration of the tool hardness, toughness, microstructure, and cutting parameters.

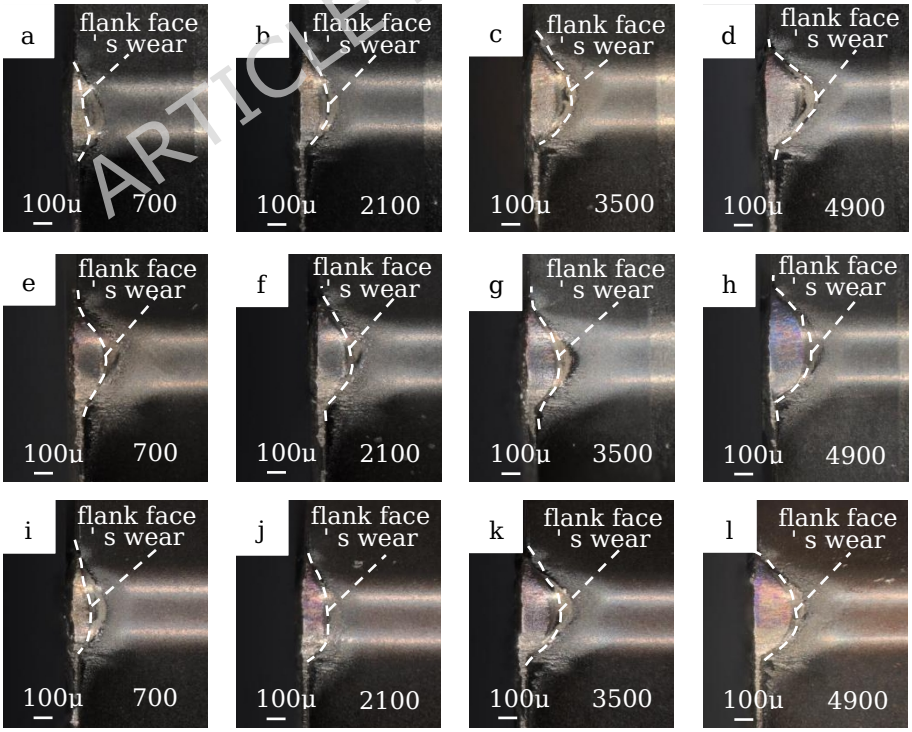

Fig.7 (a-d) tool B, (e-h) tool A, (i-l) tool C flank wear process

Analysis of the flank face wear in Fig. 7 demonstrates that during the

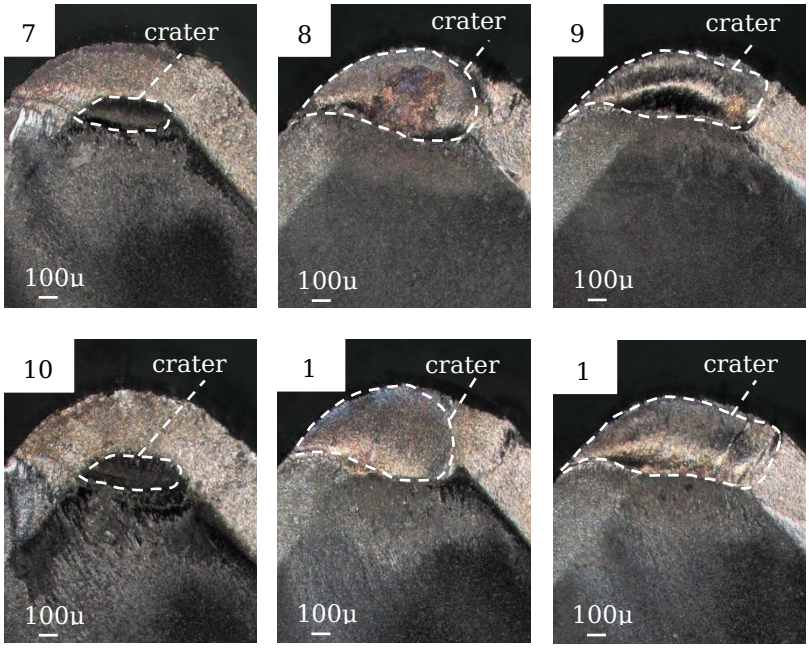

Fig.8 Test 7-12 groups of rake face wear

initial wear stage, tool A exhibits the most severe wear, followed by tool C, whereas tool B shows relatively minor wear. With an increase in the cutting length (up to 4900 m), the wear resistance of specimen C deteriorated significantly, reaching the maximum wear volume. This indicates adverse alterations in the material properties or microstructure during prolonged cutting, and all tools display elongated wear zones with typical abrasive wear characteristics. As the wear width progressively expanded, the length remained constant. Notably, the wear morphology evolves from initial linear strips to semi-lunar shapes, primarily extending along the rear and lateral flank directions. The most severe wear occurs at the tool tip centerline, diminishing toward the cutting-edge peripheries – attribuTab. to elevated cutting forces and stress concentrations at the tip midline, thereby accelerating material failure.

4.3Tool Wear Morphology Analysis

To characterize the tool wear morphology distinctly, tool B with superior cutting performance was selected for rake and flank face analysis. Fig. 8 depicts the rake face morphology of the tool B (groups 7-12) upon reaching the bluntness criterion (VB =0.2mm). Analysis reveals three wear morphology categories:1）groups 7 & 10: Minimal rake face wear, primarily featuring an elliptical wear zone concentrated away from the cutting edge;2） Groups 8 & 11: Crater wear extending to the cutting edge, forming droplet-shaped planar wear concentrated at the tool tip;3）Groups 9 & 12: Stripe-like crater wear diffusion to the cutting edge with greater depth at the central zone versus periphery.This classification demonstrates progressive evolution of wear morphology during cutting, suggesting a combined wear mechanism involving adhesion, abrasion, and diffusion.

Fig. 9 depicts the flank face morphology of cutter tool B upon reaching the bluntness standard (VB = 0.2mm) under 7-12 sets of test conditions.

Systematic analysis identified three typical modes of flank face wear, analogous to those on the rake face. The first type, corresponding to groups 7 and 10, exhibited a crescent-shaped wear land. Wear was most severe at the tool tip and diminished along the cutting edge towards both sides. As shown in Fig. 9(7), a transition zone between the worn and unworn areas showed the same trend of decreasing wear severity, similar to the first type of rake face wear, indicating that adhesive wear was the dominant mechanism at this stage. The second type, corresponding to groups 8 and 11, displayed significant asymmetry. Wear was more severe on one side of the flank, forming a distinct protrusion within the wear region. The width of this protrusion was 0.5 to 1 times that of the entire wear region, and it was accompanied by furrows. This protrusion was located on the feed side of the tool, which experienced more severe wear due to direct contact with the workpiece (see Fig. 9(11)). The third type, corresponding to groups 9 and 12, was characterized by an elongated, band-shaped wear land with a nearly uniform width. Unlike the previous types, this wear region contained evenly distributed furrows. These morphological characteristics suggest that the dominant wear mechanism transitioned to abrasive wear, and the wear process exhibited distinct steady-state features. The progression observed among these three morphologies reveals that as cutting progressed, the wear mechanism on the flank face of tool B transitioned from adhesive to abrasive wear, with local stress concentration significantly influencing the spatial distribution of the wear morphology.

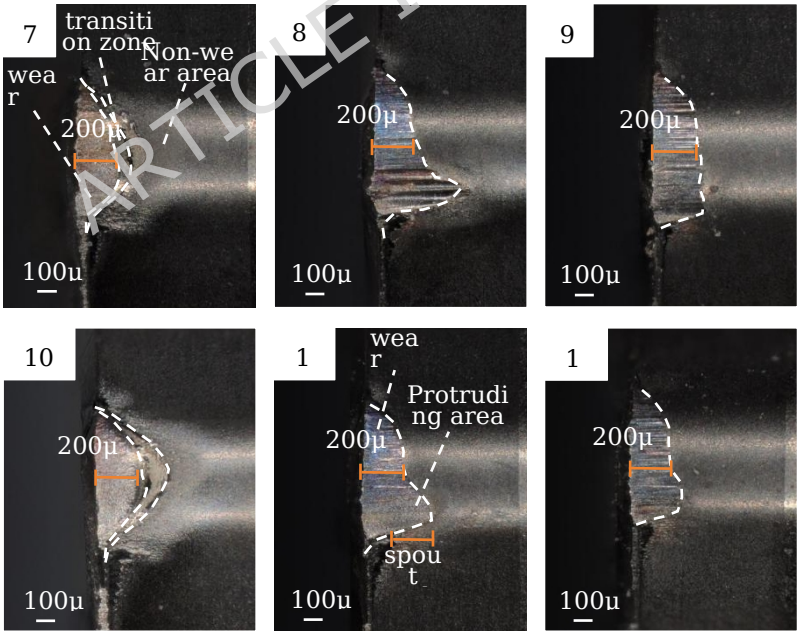

Fig.9 Test 7-12 groups of flank face wear

4.4Wear mechanism

4.4.1Abrasive wear

As a primary mechanism of tool failure, abrasive wear fundamentally originates from the micro-cutting effects exerted by hard-phase particles

within the workpiece matrix on the tool surface. Fig. 10 depicts the micromorphology of the flank faces during the cutting of ductile iron for experimental groups 7, 8, and 9. The analysis indicates that, for all tools except tool A, flank wear exhibits a significant dependence on cutting speed: as the speed increases, scratches and grooves emerge on the tool surfaces and progressively broaden and deepen. This trend is attributed to a thermo-mechanical coupling effect. Elevated cutting speeds substantially increase the temperature in the cutting zone. Although this induces thermal softening of the workpiece material, the reduced contact time at higher speeds prevents this softening from fully compensating for the abrasiveness of the hard-phase particles.

A comparison between tool A (high cBN content, >80%) and tool B reveals that the metal-bonded tool A demonstrated superior resistance to abrasive wear compared to the cermet-bonded tool B. When comparing tool B and tool C at lower speeds (<367m/min), tool C's flank face showed no scratches or furrows, while tool B exhibited only slight wear. However, at a high cutting speed of 573 m/min, distinct furrows appeared on both tools. Those on tool B were fine and shallow, whereas Tool C developed deep and broad grooves. The more severe wear in tool C is attributed to its lower cBN content (60%–65%), higher binder fraction, and consequent relative softness, which made it more susceptible to abrasion by the hard particles. Consequently, the ranking of the three tools in terms of abrasive wear resistance is: tool A > tool B > tool C.

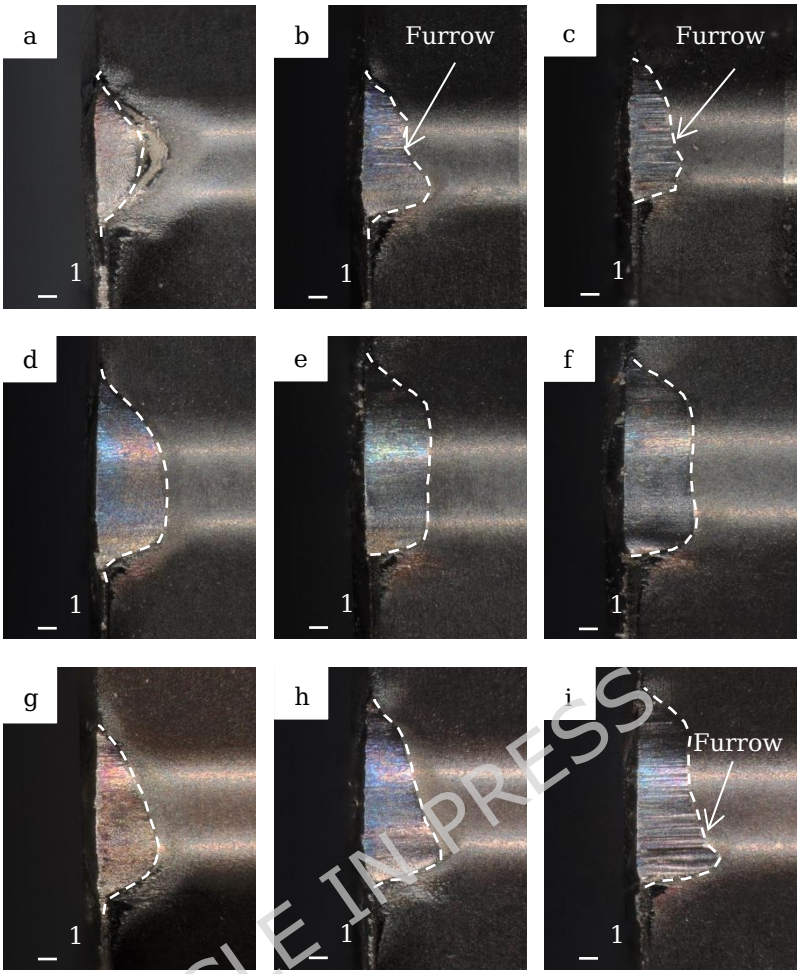

Fig.10 (a-c) No.2 tool, (d-f) No.1 tool, (g-i) No.3 tool wear morphology

4.4.2Chemical wear

Chemical wear refers to chemical reactions between the tool material and workpiece matrix or environmental medium during high-temperature cutting processes. This failure mechanism induces the degradation of surface integrity and material loss. To further elucidate the wear mechanism, specimens from test group 2 were subjected to energy-dispersive spectroscopy (EDS) analysis, comparing elemental composition variations in the unbonded regions before and after cutting (Tab. 6).

Tab.6 Tool element changes before and after cutting

Element	Tool A		Tool B		Tool C	
	Before （Atomic%）	After （Atomic%）	Before （Atomic%）	After （Atomic%）	Before （Atomic%）	After （Atomic%）
B	47.62	37.43	44.67	42.42	39.38	29.51
N	37.95	33.84	31.12	26.89	30.58	25.86
C	6.58	12.73	10.96	12.000	10.91	13.63
O	2.72	10.18	5.79	12.53	7.54	19.56
Al	0.98	2.54	3.88	3.59	3.45	3.60

Ti	0.16	2.47	3.13	2.58	7.83	5.71
W	0.73	0.08	0.29	0.23	0.25	0.19
Co	2.85	0	0.16	0	0.05	0.07
Fe	0	0.67	0	0.19	0	0.50
Si	0	0.07	0	0.28	0	0.61

By comparing the elemental changes before and after the cutting process of the three tools, it was observed that the oxygen (O) element in the unbonded area increased significantly after cutting, suggesting the occurrence of chemical wear and oxide formation in this area. Simultaneously, the boron (B) and nitrogen (N) contents decreased, which implies that cubic boron nitride (cBN) was oxidized to produce boron trioxide (B_2O_3) and nitrogen gas (N_2) during the cutting process, and nitrogen escaped from the tool surface, leading to the formation of pits. Among the three tools, the oxygen (O) element changed most significantly before and after cutting, indicating that the chemical wear of Tool C was the most severe.

Tab. 7 Comparison of tool elements(at.%)

Element	Tool A			Tool B			Tool C		
	V=188 m/min	V=294 m/min	V=459 m/min	V=188 m/min	V=294 m/min	V=459 m/min	V=188 m/min	V=294 m/min	V=459 m/min
B	44.28	29.83	38.61	42.42	29.97	42.46	29.51	8.00	41.70
C	6.59	21.30	15.91	12.00	22.45	11.55	13.63	14.83	8.71
N	35.07	29.20	34.59	26.89	28.32	33.67	25.86	30.00	32.84
Ti	0	0	0	2.58	2.32	2.48	5.71	5.79	5.19
Al	1.80	1.07	1.27	3.59	3.56	3.74	3.60	9.84	2.60
O	7.26	13.55	5.85	10.53	12.44	5.68	19.58	26.67	8.36
Fe	0.83	1.16	0.21	0.19	0.64	0.12	0.5	1.54	0.22
Co	3.19	2.56	2.44	0	0.08	0.09	0.07	0.50	0
Si	0.16	0.22	0	0.28	0	0	0.61	0.79	0
Mg	0	0	0	0.89	0	0	0.96	1.32	0.23

Tab.7 presents the elemental distribution data from the wear scar after cutting in the first, second, and third sets of tests (at corresponding cutting speeds of 188, 294, and 459m/min). The analysis indicated that the cutting speed had a significant influence on the chemical reactions on the tool surface. When the cutting speed was increased to 294 m/min, the oxygen (O) content reached a peak, while the boron (B) content decreased to its lowest value. This suggests that the boride phase underwent a vigorous oxidation reaction (e.g., $4B + 3O_2 \rightarrow 2B_2O_3$) under these conditions. When the cutting speed was further increased to 459 m/min, the carbon (C) content was markedly reduced, which is directly associated with the oxidation of the carbon-rich binder in tool C (e.g., $C + O_2 \rightarrow CO/CO_2$).

Combined with the microscopic morphology observed in Fig. 8, an

increase in cutting speed causes the heat-affected zone (dark area) and the oxidation product enrichment zone (bright area) to first expand and then contract. When the cutting speed exceeded 294m/min, the bright-zone area diminished significantly, consistent with accelerated oxide spalling due to oxidation rates surpassing diffusion rates at high velocities. This oxidation-spalling interaction directly reduces the interfacial bonding strength between the cBN particles and the binder matrix, inducing particle-delamination wear.

Crucially, tool C maintained its peak oxygen content during cutting. This correlates with its high binder content enhancing oxidative activity: at elevated temperatures, binder elements (Al, Co, C) undergo selective oxidation forming porous oxides (Al_2O_3, CoO), drastically weakening interfacial cohesion and triggering cBN particle spallation. This oxidation-dominated mechanism explains the dramatic reduction in wear

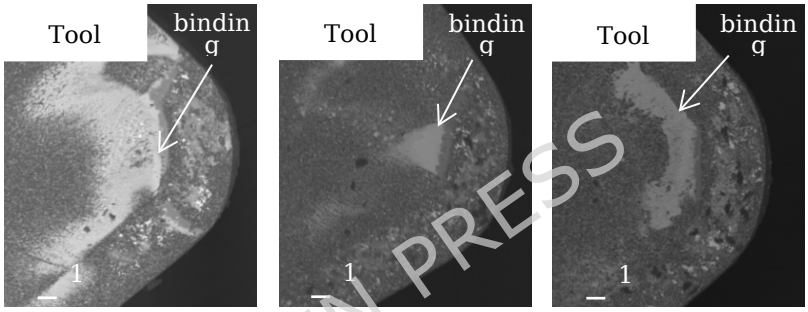

Fig.11 Tool binder

resistance of tool C under high-speed cutting.

4.4.3Adhesive wear

Adhesive wear is a typical failure mode that results from molecular/atomic adhesion at the contact interface between the tool and workpiece during the cutting process. Fig. 11 presents the distribution characteristics of the binder phase on the rake face of the three tools in test group 1 after cutting. Research indicates that, under the same cutting parameters, distinct binder layers are formed on the surfaces of the three tools. Among these tools, the binder phase on the rake face of tool B covers the largest area. The crater area exhibits a characteristic pit morphology formed by the periodic tearing of the binder layer, which is consistent with the typical wear characteristics under the bonding - tearing coupling mechanism.

Energy-dispersive spectroscopy (EDS;see Tab.8) indicated that an interaction between ductile iron and the tool binder occurred during the cutting process. Under high-temperature and high-pressure conditions, the metal elements (Al, Ti) in the binder on the tool surface and the Fe and C elements in the workpiece diffuse and migrate, resulting in the formation of intermetallic compounds (e.g., Fe–and Al TiC) at the contact interface. Simultaneously, the oxidation reaction (enrichment of O) causes periodic fluctuations in the interface bonding strength, ultimately resulting in

periodic tearing and redeposition of the bonding layer. This adhesive - tearing interaction mechanism directly contributes to the formation of a characteristic adhesive wear morphology on the tool rake face, and the

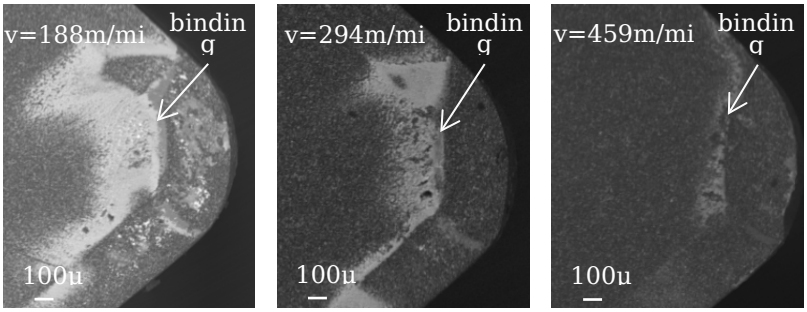

Fig.12 Tool binder at different cutting speeds

severity of this phenomenon is closely associated with the tool binder system. Tool B is more prone to softening the binder phase under the influence of cutting heat. This softening aggravates the adhesion and tearing behavior of ductile iron and is directly associated with the typical pit morphology observed in the crater area.

Tab. 8 Binder element distribution(at.%)

Element	Tool A	Tool B	Tool C	Element	Tool A	Tool B	Tool C
C	0.82	19.64	13.65	Fe	63.94	51.47	36.76
O	26.68	24.24	33.21	Mg	1.08	/	/
Si	5.48	3.30	2.35	Al	/	/	1.53
Ti	/	1.34	10.19				

This study investigated the distribution characteristics and elemental composition of adherents on tool B, selected for its superior cutting performance, under varying cutting speeds. The corresponding test groups (Groups 1–3) were operated at 188, 294, and 459 m/min, respectively. The results are shown in Fig. 12 and Tab. 9.

Fig. 12 shows that as the cutting speed increases, the coverage rate of the bonded phase on the rake face of the tool exhibits a decreasing trend. Under low-speed cutting conditions ($v < 294$ m/min), the thermal effect accumulation at the tool–workpiece contact interface is insufficient, leading to the following:1) the probability of diffusion and migration of the workpiece material (elements Fe and C) to the tool surface increases significantly.2)The growth rate of the oxide film on the tool surface (mainly containing phases such as Al_2O_3 and TiO_2) is lower than the mechanical removal rate, and its integrity is insufficient to suppress the plowing effect of the chips.3)This thermo - mechanical coupling mechanism causes the workpiece material to form a continuous adhesive layer on the tool's rake face, ultimately inducing a severe adhesive wear morphology characterized by the expansion of the crater.

Tab.9 reveals that within the experimental parameter range (v =

188-459m/min), the elemental composition of the binder phase on the tool's rake face remains stable, predominantly composed of Fe, O, and C. This indicates that variations in cutting speed do not alter the phase characteristics of the binder phase. This reduction in binder coverage can be ascribed to the alteration of the thermomechanical coupling mechanism under high-speed cutting conditions. As the cutting speed increases, the strain rate at the tool-workpiece contact interface increases, which results in: 1) a decreased probability of the diffusion and migration of the workpiece material to the tool surface; 2) the growth rate and mechanical removal rate of the oxide film reach a dynamic equilibrium, and its integrity is adequate to suppress chip plowing. The transformation of the interfacial interaction mechanism causes the formation rate of the binder phase to be lower than the stripping rate, ultimately resulting in a significant reduction in binder phase coverage. This phenomenon validates that the adhesive wear behavior is governed by the competitive mechanism between the evolution of oxide film integrity and the mechanical peeling effect within a specific speed range.

Tab. 9 Binder element distribution(at.%)

Element	V=188m/min	V=294m/min	V=459m/min	Element	V=188m/min	V=294m/min	V=459m/min
C	19.64	21.06	20.77	Fe	51.47	52.08	31.30
O	24.24	20.39	32.91	Co	/	0.19	/
Si	3.30	2.92	3.58	Al	/	/	3.01
Ti	1.34	0.73	0.70				

5.Analysis and optimization of cutting parameters

5.1Life Analysis of Orthogonal Test

Cutting tests were carried out on three types of tools, and the results were recorded. The tool lives obtained from the multiple cuttings are listed in Tab.10. Because the test parameters of each group were different, the cutting time when the flank face of the tool reached the wear-blunt standard was recorded as the final data to represent the tool life.

Tab.10 Tool life when cutting ductile iron

Experiment group	Tool A life /min			Tool B life /min			Tool C life /min		
	1	2	3	1	2	3	1	2	3
1	42.97	42.60	43.30	51.29	50.90	51.59	53.72	53.26	54.24
2	3.82	3.61	4.21	5.07	4.65	5.23	9.86	9.50	10.06
3	0.84	0.77	0.99	1.74	1.58	1.87	1.98	1.88	2.07
4	7.61	7.33	7.92	10.39	10.16	10.76	11.10	10.94	11.44
5	1.15	1.07	1.24	2.51	2.34	2.76	3.98	3.79	4.25
6	0.77	0.70	0.87	0.95	0.88	1.05	1.85	1.78	2.04
7	3.42	3.23	3.78	15.01	14.65	15.36	8.76	8.52	9.07
8	1.36	1.21	1.54	4.26	4.11	4.51	2.42	2.26	2.52

9	0.51	0.50	0.63	1.28	1.23	1.37	1.52	1.43	1.54
10	8.67	8.41	9.04	35.78	35.30	36.02	19.48	19.24	19.97
11	1.73	1.64	1.91	3.74	3.60	3.92	4.68	4.37	4.99
12	1.09	1.03	1.23	1.30	1.23	1.39	1.97	1.87	2.11

A variance analysis method was employed to conduct an in-depth analysis of the data in Tab. 9.Subsequently,the variance analysis results and significance of the tool cutting life were obtained,as presented in Tab. 11.

Tab. 11 Analysis of variance

	Tool A			Tool B			Tool C		
	Mean Square	F	Significance	Mean Square	F	Significance	Mean Square	F	Significance
V	575.303	14.224	0.000	575.303	14.224	0.000	1076.802	29.444	0.000
f	255.360	6.314	0.018	255.360	6.314	0.018	304.852	8.336	0.007
ap	405.620	10.029	0.004	405.620	10.029	0.004	476.840	13.039	0.001
	R^2=0.757，After AdjustmentR2=0.697；			R^2=0.973，After adjustmentR2=0.966；			R^2=0.858，After adjustmentR2=0.822；		

It can be seen from the results of Tab. 10, only the cutting depth (ap) of tool B has a significant effect on tool life (greater than 0.05), and the remaining significance values are less than 0.05. This shows that the cutting speed and feed rate of tool B have a significant effect on tool life, whereas the cutting depth has no significant effect. The cutting speed, feed rate, and cutting depth of other tools have significant effects on tool life. The F statistics of the whole model were 141.688, 12.495, and 24.085, respectively, and the significance was 0.000, indicating that the analysis of variance model was significant. The R square are 0.973, 0.757, and 0.858, respectively, indicating that the cutting life of the tool is explained by the cutting speed, feed rate, cutting depth, and their interaction, which are 97.3%, 75.7%, and 85.8%, respectively.When the significance is equal, the F value can also reflect the primary and secondary relationship of the influence of each factor. By comparing the size of the F value, it can also be seen that the order of influence of each factor in tool B cutting is v＞f＞ap, tool A and tool C are v＞ap＞f.

5.2Establishment of Regression Model

Using the results of the orthogonal experiment, the functional relationship between each factor and the index was established using a regression model, and the relationship between the cutting parameters and tool life was explored. Based on the above conclusions on the relevant laws, this study chose the multiple linear regression model, and its basic expression is:

$$\hat{y} = b_0 + b_1 x_1 + b_2 x_2 + \cdots + b_p x_p + \varepsilon \quad (3)$$

In the formula, $\hat{y}$ is the index of the experimental results, $x_1 \cdot x_2 \cdot \ldots \cdot x_p$ is p factors, $b_0 \cdot b_1 \cdot \ldots \cdot b_p$ is $p+1$ regression coefficient and ε is random error.

It can be seen from the results of the fourth section that in order to ensure the better life and cutting efficiency of the tool, the cutting efficiency should be selected in the range of less than 20 cm^3 / min, and the cutting speed is less than 367m / min.Therefore, this paper only calculates the regression equation of the tool life when the cutting speed is less than or equal to 367m / min.

By importing all the data in Tab. 8 into the regression analysis module in the data science analysis platform, the regression model equations of the three types of cutting tools for ductile iron were obtained as follows:

$$\begin{cases} \hat{y} = 105.126 - 0.120X - 162.217Y - 100.742Z & \text{Tool A} \\ \hat{y} = 100.372 - 0.203X - 115.583Y - 26.158Z & \text{Tool B} \\ \hat{y} = 127.287 - 0.163X - 176.600Y - 108.217Z & \text{Tool C} \end{cases} \tag{4}$$

The regression equation of tool B cutting ductile iron is selected by studying the tool life of 4.4 section.After establishing the regression model equation, it is necessary to test it to evaluate its fitting effect and predictive ability.In this section, we will use the proportion of the regression square sum SSR in the total square sum SST to judge the closeness between the regression model and the actual situation. The proportion is generally expressed by the dimensionless symbol R^2, which is calculated as follows:

$$R^2 = \frac{SSR}{SST} = \frac{\sum_{i=1}^{n} (\hat{y}_i - \bar{y})^2}{\sum_{i=1}^{n} (y_i - \bar{y})^2} \tag{5}$$

The significance of the regression equation was less than 0.001, indicating that it was significant. The calculated adjusted R^2 was 0.651, and the remaining tool regression equation R^2 was greater than 0.6. R^2 is an important index for judging the goodness of linear regression. The value range is 0-1. Generally, when R^2 is greater than 0.6, the fitting effect is better. Therefore, the fitting degree of the regression equation obtained in this study is better and can be used to predict the tool life.

5.3 Real-time Tool Life Prediction

5.3.1 Integrated Real-time Parameter-based Life Prediction Model

During the real-time prediction phase, cutting parameters (cutting speed, feed rate, depth of cut) are captured in real-time via sensors.These parameters are input into the corresponding multiple linear regression model to calculate the predicted life under current conditions.To simplify the real-time life prediction model, the three tool life prediction models from equation (4) are now transformed into the following form:

$$T_{total}(t_i) = b_0 + b_1 \times v_c(t_i) + b_2 \times f(t_i) + b_3 \times a_p(t_i) + e(t_i) \tag{6}$$

t-timestamp,indicating that this set of parameters was collected at a specific point in time；$v_c(t)$-cutting speed at time t(m/min)；$f(t)$-feed rate at time t(mm/r)；$a_p(t)$-cutting depth at time t(mm)；$T_{\text{total}}(t)$-theoretical total lifespan based on parameter prediction at time t(min)；β_0-regression intercept(min)；β_1-cutting speed regression coefficient(min^2/m)；β_2-regression coefficient for feed rate (min·r/mm)；β_3-cutting depth regression coefficient (min/mm)；$\varepsilon(t)$-model residual at time t(min)；

5.3.2 Dynamically Updated Remaining Service Life Calculation Model

The tool total life prediction model based on equation (6),combined with the system's real-time recording of effective cutting time via indicator function $I(\tau)$ as per equation (7),enables calculation of the tool's remaining service life under current cutting parameters using equation (8).The system dynamically monitors changes in cutting parameters,reca culating the predicted life whenever parameters alter.Furthermore,to present the tool's health status more intuitively,the remaining life is converted into a health percentage, as demonstrated in equation (9).

$$T_{used}(t_i)=\int_0^{t_i} I(t)dt \approx \sum_{k=1}^{N} t_k \quad (7)$$

$$RUL(t_i)=T_{total}(t_i)\times Health(t_{i-1})-T_{used}(t_i) \quad (8)$$

$$Health(t_i)=\frac{RUL(t_i)}{T_{total}(t_i)}\times 100\% \quad (9)$$

$RUL(t)$-residual useful life at time t, indicating the remaining operational time of the tool in its current condition (min)；$T_{used}(t)$-cumulative effective cutting time up to time t (min).Where $I(\tau)$ denotes the indicator function, equal to 1 when the machine tool is in a cutting state,and 0 otherwise;Health(%)-tool health coefficient (initial value 100%),representing the ratio of remaining usable life to total life under a given set of characteristic parameters.

5.3.3 Empirical Analysis of the Real-Time Tool Life Prediction Process

The real-time tool life prediction process is illustrated in Fig.13.During the initial phase, machine tool sensors continuously gather cutting parameters (cutting speed, feed rate, cutting depth) and effective cutting duration.Subsequently, these parameters are input into the predictive model to calculate the theoretical total life expectancy based on the health coefficient under current conditions.Thereafter, the remaining service life and health status are determined by subtracting the cumulative cutting time from the theoretical total life expectancy.Finally,the monitoring system compares the health status against predefined thresholds to determine whether to issue an early warning alert.

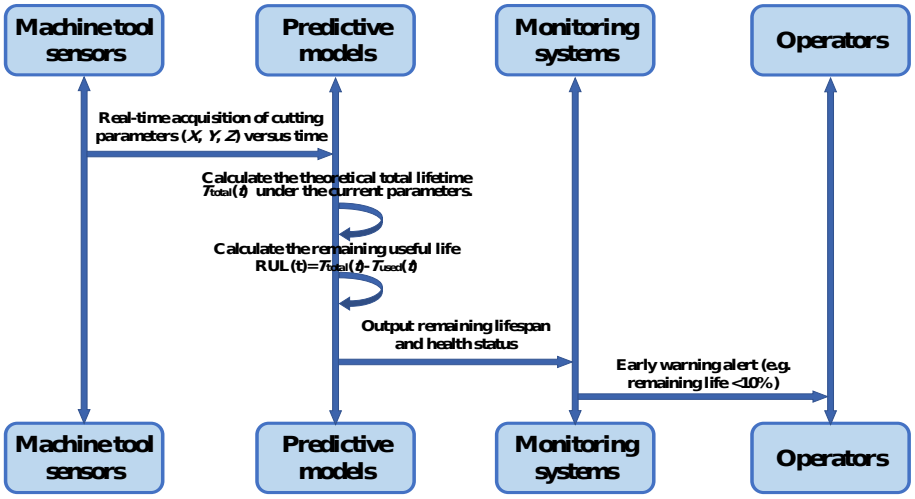

Fig.13 Real-time tool life prediction flowchart

Tab. 12 presents the predicted tool life of tool A under various cutting parameters.During the initial cutting process,the machine tool sensor recorded cutting parameters (cutting speed 188m/min, feed rate 0.2mm/rev, feed depth 0.4mm),with a health factor of 100%.Based on the multiple linear regression equation (equation (4)-①),the predicted remaining life was 9.83 minutes;Simultaneously,the system recorded the effective cutting time as 1 minute via equation (7). Substituting into equations (8) and (9) yields a remaining life of 8.83 minutes and a post-cutting health factor of 89.82%.Following threshold comparison,the system determined the tool condition to be satisfactory.Subsequent cutting operations proceeded sequentially until the sixth cut,when the health factor abruptly dropped to 5.96%,triggering an early warning prompting the operator to replace the tool.

Tab. 12 Predicted tool life of tool A under different cutting parameters

Number of cuts	1	2	3	4	5	6
Cutting speed(m/min)	188	190	240	210	300	100
Feed rate（mm/r）	0.2	0.1	0.2	0.3	0.15	0.2
Depth of cut（mm）	0.4	0.4	0.3	0.2	0.2	0.3
Pre-cutting health coefficient(%)	100.00	89.82	70.45	48.49	30.49	22.37
Predicted total service life based on health factor	9.83	23.18	9.62	5.39	7.51	6.81
Cutting time	1	5	3	2	2	5
Remaining service life	8.83	18.18	6.62	3.39	5.51	1.81
Health coefficient after cutting(%)	89.82	70.45	48.49	30.49	22.37	5.96
Health status	Good	Good	Good	Good	Good	Warning

6. Conclusion

This study, focusing on ductile iron materials widely employed in automotive manufacturing, compares the wear behaviour of three distinct tool materials during machining processes. The core conclusions drawn aim to provide optimisation guidance for practical production, thereby enhancing machining efficiency and tool service life:

1)Tool wear results from abrasive, chemical, and adhesive wear.At high cutting speeds (v > 367m/min), abrasive wear dominates. Titanium carbide–bonded tools with lower cBN content outperformed high-cBN metal-bonded tools under high-speed conditions, extending tool life by up to 80%.

2）Orthogonal experiments and regression analysis (model $R^2 > 0.85$) confirmed tool B as the optimal choice for machining ductile iron. Its optimum cutting efficiency is 15.04 cm^3/min, achieved with the following parameter combination: cutting speed v = 188 m/min, feed rate f = 0.2 mm/r, and cutting depth ap = 0.4 mm. This condition achieves the optimal balance between tool life and material removal rate.

3）Cutting speed most significantly affects tool life. For Tool B, parameter influence follows v > f > ap, while for the other tools it is v > ap > f, highlighting material-dependent sensitivity.

4）A real-time tool life prediction method based on multiple linear regression was proposed and validated. By continuously acquiring cutting parameters, it dynamically forecasts tool life and evaluates health status online. Empirical results demonstrate this method effectively monitors tool wear progression and issues early warnings before life depletion, providing a reliable technical solution for intelligent predictive tool maintenance.

5）The results can be directly applied to batch production of automotive parts (e.g., drive motor housings). Using optimized tools and parameters extends tool life, reduces change frequency, and—combined with real-time monitoring—improves production line efficiency and lowers costs.

References:

[1] Muthuswamy P .A novel wiper insert design and an experimental investigation to compare its performance in face milling[J].Advances in materials and processing technologies, 2022.

[2] Muthuswamy, P. A novel wiper insert design and an experimental investigation to compare its performance in face milling. Advances in Materials and Processing Technologies, 8(sup4), 2070–2085.

[3]Zou Q, Dong P, Li Y, et al. Preparation and characterization of PcBN composites with high-entropy ceramic bonding. Diamond and Related Materials, 2023, 131: 109591.

[4]Geng X, Xu J, Yu Z. Comparative analysis of cutting performance and dead metal zone in ductile iron machining using PCBN chamfered tools with and without micro-pit texture [J]. Journal of Manufacturing Processes, https://doi.org/10.1016/j.jmapro.2025.05.047

[5]Uhlmann E, Fuentes J A O, Keunecke M. Machining of high-performance workpiece materials with CBN coated cutting tools. Thin Solid Films, 2021, 736: 138915.

[6] Geng X, Xu J, Yu Z. Comparative analysis of cutting performance and dead metal zone

in ductile iron machining using PCBN chamfered tools with and without micro-pit texture. Journal of Manufacturing Processes, 2025, 128: 599-614. DOI:10.1016/j.jmapro.2025.05.047

[7] Peicheng M, Chen C, Guang J, et al. Effect of tungsten content on microstructure and mechanical properties of PcBN synthesized in cBN-Ti-Al-W system. International Journal of Refractory Metals & Hard Materials, 2020, 87: 105138.

[8] Tu L , Tian S , Xu F ,et al.Cutting performance of cubic boron nitride-coated tools in dry turning of hardened ductile iron[J].Journal of Manufacturing Processes, 2020, 56:158-168.DOI:10.1016/j.jmapro.2020.04.081.

[9] Xie Hui. Interfacial structure and properties of polycrystalline cubic boron nitride cutting tool materials[D]. China University of Mining and Technology (Beijing), 2022.DOI:10.27624/d.cnki.gzkbu.2022.000020.

[10] Jian Li. Preparation of high-performance polycrystalline cubic boron nitride tool and its cutting performance research [D]. Zhengzhou University,2018.

[11] Boing L S R B .Prediction of PCBN tool life in hard turning process based on the three-dimensional tool wear parameter[J].The International Journal of Advanced Manufacturing Technology, 2020, 106(1a2).

[12] Khadka S , Rahman Rashid R A , Stephens G ,et al.Predicting cutting tool life: models, modelling, and monitoring[J].International Journal of Advanced Manufacturing Technology, 2025.

[13]Wu, Mingyang.Wei, Min ,et al.Simulation analysis of flank wear and tool life prediction for cutting superalloy under high-pressure cooling.Surface Topography.Metrology and Properties[J]. Volume 10, Issue 3, id.035035, 10 pp.

[14]Muthuswamy, Padmakumar. Comparison of Machining Forces, Power Consumption, and Specific Cutting Energy in Tools with Grooved Cutting Edges for Sustainable Manufacturing. Advances in Materials and Processing Technologies 11 (3): 1922–36. doi:10.1080/2374068X.2024.2402969.

[15] Muthuswamy P .Influence of micro-geometry of wiper facet on the performance of a milling insert: an experimental investigation and validation using numerical simulation[J].Sadhana, 2022, 47(3):13.DOI:10.1007/s12046-022-01912-4.

[16] Shree M S , Raguraman K , , Velan M V G ,et al. Experimental Investigation on Effect of High Pressure Coolant with Various Cutting Speed and Feed on Cutting Force and Tool Life in Cylindrical Turning of AISI 1060 Steel Using Carbide Insert[J]. Social Science Electronic Publishing[2025-12-11]. DOI:10.2139/ssrn.3963657.

[17] Peicheng M, Chao C, Jiarong C , et al. Effect of sintering temperature on synthesis of PcBN in cBN-Ti-Al-W system[J]. Diamond Related Materials, 2020, 103(C): 107714-107714.

[18] Qin Mingli, Qu Xuanhui. Characteristics, preparation and application of Al(AlN) nitride ceramics[J]. Ceramic Engineering, 2000, 34(4): 39-42.

[19] Grzesik W, Kiszka P, Kowalczyk D, et al. Investigation of the machining process of spheroidal cast iron using cubic boron nitride (cBN) tools[J]. Metalurgija, 2014, 53(1): 33-36.

[20] Grzesik W, Kiszka P, Kowalczyk D, et al. Machining of nodular cast iron (PF- NCI) using cBN tools[J]. Procedia CIRP, 2012, 1: 483-487.

Funding

This research was supported by the Ningbo Key Research and Development Programme (2023Z039), the Ningbo Yongjiang Talent Project for Young Innovative Talents (2024A-334-G), and the 2023 China Academy of Mechanical Engineering Innovation Leading Talent Innovation Team Project, and was funded by Science Research Project of Hebei Education Department,grant number QN2023238.

Data availability

All data generated or analysed during this study are included in this published article (and are presented in the main Figures and Tables).

Author contributions

P.W. and Y.J. were responsible for the conception, supervision, review, and editing of the study. X.L. was primarily responsible for literature research and organisation. H.Y. made important contributions to the implementation of the experiment. Y.Z. is responsible for the manuscript editing. All authors participated in the discussion of the results and contributed to the final draft.

Competing interests

The authors declare no competing financial interests.

Acknowledgements

This study was supported by the Ningbo Key Research and Development Programme (2023Z039), the Ningbo Yongjiang Talent Project for Young Innovative Talents (2024A-334-G), and Funded by Science Research Project of Hebei Education Department（QN2023238）. The authors also thank the reviewers for their valuable comments and suggestions.